frontiers | Frontiers in Mechanical Engineering

TYPE Original Research
PUBLISHED 30 September 2024
DOI 10.3389/fmech.2024.1464692

Check for updates

OPEN ACCESS

EDITED BY
Kai Wang,
Hunan University, China

REVIEWED BY
Yaopeng Chang,
Changsha University of Science and Technology, China
Qiang Wang,
Hunan University, China
Xia Shuyan,
Guangzhou University, China

*CORRESPONDENCE
Mohammad A. Abido,
mabido@kfupm.edu.sa

RECEIVED 14 July 2024
ACCEPTED 16 September 2024
PUBLISHED 30 September 2024

CITATION
Shamseldin A, Abido MA and Alofi A (2024) AI-driven optimization of dynamic vibration absorbers with hydraulic amplifier and mechanical inerter integration.
Front. Mech. Eng. 10:1464692.
doi: 10.3389/fmech.2024.1464692

COPYRIGHT
© 2024 Shamseldin, Abido and Alofi. This is an open-access article distributed under the terms of the Creative Commons Attribution License (CC BY). The use, distribution or reproduction in other forums is permitted, provided the original author(s) and the copyright owner(s) are credited and that the original publication in this journal is cited, in accordance with accepted academic practice. No use, distribution or reproduction is permitted which does not comply with these terms.

AI-driven optimization of dynamic vibration absorbers with hydraulic amplifier and mechanical inerter integration

Ahmed Shamseldin[1], Mohammad A. Abido[2]* and Abdulrahman Alofi[1,3]

[1]Mechanical Engineering Department, King Fahd University of Petroleum and Minerals, Dhahran, Saudi Arabia, [2]Electrical Engineering Department, King Fahd University of Petroleum and Minerals, Dhahran, Saudi Arabia, [3]Interdisciplinary Research Center for Intelligent Manufacturing and Robotics, King Fahd University of Petroleum and Minerals, Dhahran, Saudi Arabia

Dynamic vibration absorbers (DVAs) have been widely employed in vibration suppression applications for decades. While DVAs offer an effective solution, they are limited by the need for a high mass ratio between the DVA and the primary system to achieve significant vibration attenuation. To overcome this, researchers have introduced lever mechanisms, allowing for enhanced vibration suppression without increasing the mass ratio. However, levers, commonly used as amplification mechanisms, suffer from high inertia and limited amplification, particularly in larger applications. Another limitation is when DVAs are employed for energy harvesting as a secondary objective, they exhibit high sensitivity to system parameter variations, requiring extensive optimization. Various optimization techniques have been applied to DVAs for multi-objective optimization, including fixed-point theory, which is complex and requires intensive mathematical derivation, and simple metaheuristic techniques such as genetic algorithms (GA). This study proposes four novel DVAs using a hydraulic amplifier (HA) to address the limitations of traditional lever mechanisms and a mechanical inerter to improve the vibration damping. Also, multi-objective optimization was performed using particle swarm optimization (PSO) which is considered innovative in this application and compared with commonly used genetic algorithms (GA). The governing equations were derived using Newton's second law and solved numerically with the Runge-Kutta method. An AI-based approach was utilized for HA design. The results show that integrating HA and mechanical inerters significantly enhances vibration attenuation and broadens the frequency response. Additionally, the location of the mechanical inerter is critical in reducing vibration amplitude. Also, the multi-objective PSO outperforms GA in solution diversity and quality. The proposed integration of HA in DVAs offers potential applications across various engineering fields.

KEYWORDS

dynamic vibration absorber, energy harvesting, particle swarm optimization, artificial neural networks, mechanical inerter, hydraulic amplifier

Introduction

Vibration control mechanisms are typically employed to adjust and attenuate vibrations within a system, utilizing both passive and active control methodologies (Balaji and Karthik SelvaKumar, 2020). One such innovative approach is the DVA. The DVA design incorporates an additional mass that interacts with the primary system. The resultant system will exhibit two resonance frequencies instead of one. However, at the primary system's resonance frequency, the excitation will be minimized. This differs from conventional damping methods, which seek to dissipate vibration energy by using dampers that convert it into heat through fluid friction. DVAs have been the subject of extensive research in the last decades (Martins et al., 2020a; Auleley et al., 2021; Sun et al., 2023). Initially, DVA is primarily employed to attenuate vibrations at the resonance frequency of the primary system. Then, several proposed designs aim to expand the frequency range of DVA absorption, such as the system introduced in (Wang et al., 2019). However, the effectiveness of DVA at non-resonance frequencies is inherently constrained by the mass ratio between the primary and secondary systems. Engineers often seek to overcome these limitations by utilizing amplification techniques to adjust the mass and natural frequency ratios. Su et al. (2023) proposed an innovative inerter-lever type DVA that offers superior control characteristics, making it a more efficient and feasible solution. Shen et al. (2019) introduced a model that integrates ground stiffness and amplification mechanisms, successfully reducing the maximum amplitude and broadening the effective frequency range. Similarly, Shi et al. (2022) investigated a novel DVA design featuring a lever, ground stiffness, and an inerter, achieving significant amplitude reduction and an expanded frequency range. Li et al. (2023) proposed an optimized novel Maxwell DVA, which demonstrates superior absorption performance.

In mechanical engineering, leverage systems and Hydraulic systems serve as the most common amplification mechanisms. Leverage systems encounter challenges with high inertia in systems with significant masses or large arm ratios, leading to inefficient response and control difficulties. Conversely, hydraulic systems demonstrate superior control and generate substantial force outputs in heavy systems. HA, operating on Pascal's principle of confined fluid, finds widespread application in various fields for amplifying displacement or force (Bartnicki and Klimek, 2019; Xu et al., 2021). Energy loss in HA primarily arises from friction between the fluid and pipe walls, as well as between the piston ring and the inner wall of the pipe (Qin et al., 2023). Traditionally, a mass, spring element, and damping mechanism constitute the mass-spring-damper system, forming the core of a vibration absorber. Recently, engineers have uncovered the mechanical inerter as one of the damping mechanisms. A mechanical inerter, designed to produce force proportional to the relative acceleration between its terminals, enhances system damping with minimal added mass (Jangid, 2021) Numerous studies have been dedicated to enhancing the capabilities of mechanical inerters (Zhang et al., 2020), finding applications in various DVAs to improve overall system performance. These inerter devices have found applications within various DVAs with the intent of enhancing the overall system performance. In another study, Li et al. (2022) introduced a novel DVA incorporating an inerter mass, broadening the frequency range while mitigating peak excitation levels. Alotta and Failla (2021) proposed an inerter-based DVA integrated into a rhombus truss structure, which offers mechanical amplification and facilitates frequency adjustment through geometric configuration alterations. Additionally, Barredo et al. (2020) developed an inerter-based DVA specifically designed for civil engineering structures, effectively attenuating stochastic vibrations. In addition to that the application of hydraulic systems in dynamic vibration absorbers (DVAs) has attracted significant interest among researchers. For instance, Rong et al. (2024) have developed a nonlinear gas-spring dynamic vibration absorber (NGSDVA), which exhibits broad-spectrum vibration suppression capabilities across different excitation amplitudes. Additionally, through experimental studies, Brötz et al. (2024) have designed a fluid-based dynamic vibration absorber (FDVA) specifically for automotive suspension systems, achieving a 3.5% improvement in ride comfort and a 4.3% reduction in wheel load fluctuations.

Vibrational energy harvesting involves capturing vibrational energy and converting it into usable energy (Zhou et al., 2022). This method overcomes many limitations of renewable energy sources, which often rely on specific weather or environmental conditions (Muscat et al., 2022). The primary methods of energy harvesting include piezoelectric, electrostatic, and electromagnetic (Ahmad and Khan, 2021). Piezoelectric materials, with their mechanical-electric coupling characteristics, can convert strain into voltage. Due to their ability to both dampen vibrations and harness energy, DVAs have garnered attention from numerous researchers in the context of energy harvesting. Wang et al. (2023) introduced a quasi-zero-stiffness DVA for energy harvesting and low-frequency vibration mitigation. Their model effectively dampened vibrations within the ultra-low frequency range. By optimizing DVA parameters, they observed an increase in peak power output. In a similar study, Wang et al. (2020) utilized a non-linear spring element to broaden the effective bandwidth in a dual-function vibrational apparatus (DVA), serving both energy harvesting and vibration damping purposes. Zoka and Afsharfard (2019) proposed a double-stiffness DVA for energy harvesting and vibration suppression. The proposed DVA exhibited a higher Perfection Rate (PR) parameter compared to traditional DVAs, enhancing its energy harvesting capabilities while effectively dampening vibrations.

Numerous techniques have been employed in optimizing DVAs, with two prominent methodologies taking the lead: fixed-point theory, described in (Shen et al., 2019; Baduidana and Kenfack-Jiotsa, 2022) and more recently the adoption of meta-heuristic algorithmic techniques (Kassem et al., 2021; Wang et al., 2022; Xu et al., 2024). Meta-heuristic techniques, such as GA, DE, and PSO, are stochastic methods that navigate the solution space in search of the optimal solution. These approaches prove invaluable when tackling problems characterized by immense complexity or lacking a well-defined mathematical structure, a common scenario in vibrational system optimization. Among the meta-heuristic techniques, GA, DE, and PSO are the most prevalent. DE functions as a population-based meta-heuristic method that evaluates differences among candidate solutions (Bilal et al., 2020). Renowned for its efficiency and resilience (Ahmad et al., 2022), DE generates vast volumes of optimized datasets for training

purposes and finds extensive application in engineering systems optimization, as evidenced in (Kim et al., 2019; Arthur et al., 2020). The PSO technique represents a meta-heuristic optimization approach inspired by the collective behavior of birds (Gad, 2022). In this approach, each solution dynamically adjusts its position by integrating its historical performance and the collective experiences of other solution particles (Wang et al., 2017). This mechanism allows PSO to have a distinctive capacity for enhancing both global and local exploration. PSO offers several key advantages, such as its ease of execution and minimal requirement for controlling parameters (Shami et al., 2022).

Despite the various amplification mechanisms employed in the design of DVAs, the implementation of a HA offers distinct advantages. Traditional methods, such as lever mechanisms, often necessitate high lever arm ratios for large vibration suppression, leading to larger, less efficient systems with challenges related to rigidity and high inertia. In contrast, amplification in DVAs equipped with HAs relies only on the diameter's ratio. *It provides* the capability to absorb vibrations at alternative locations, thereby enhancing design flexibility and efficiency. In addition to that, the inertia in HA-based systems can be readily adjusted by modifying the hydraulic fluid, further improving their adaptability. These characteristics position HA-equipped DVAs as superior to those utilizing traditional amplification mechanisms.

The integration of AI into vibration applications has significantly advanced the field, particularly in optimization and data training. Although existing optimization methods have shown effectiveness, they are often limited by complexity and a lack of adaptability. PSO is recognized for its efficiency and often outperforms GA in various applications. However, many researchers, such as Martins et al. (2020), have employed GA for multi-objective optimization of DVAs, while the application of PSO, as seen in the works of Song et al. (2022) and Zhe-Ming et al. (2019), has primarily focused on single-objective optimizations. However, multi-objective optimization, which aims to maximize output voltage while minimizing the maximum amplitude of the main system within a designated operating frequency range, remains underexplored. In this research, PSO and GA are used as the multi-objective optimization methods for the proposed. Then, Artificial Neural Networks (ANNs) are utilized to predict the parameters of the HA.

This research makes significant contributions by introducing the novel application of HAs in DVAs to overcome the limitations of traditional lever mechanisms. Additionally, it utilizes AI in structural dynamic systems, focusing on the multi-objective optimization of DVAs using PSO and GA, and includes a comparative analysis between the two methods. Together, these innovations offer a more adaptive and efficient approach to vibration absorption and energy harvesting. Click or tap here to enter text. Click or tap here to enter text. Click or tap here to enter text. The structure of the paper is outlined as follows: Section 2 1 presents the mathematical model of the proposed systems and describes the HA modeling and optimization using the DE algorithm to minimize friction loss and reduce pipe weight. It also includes the training process of ANN for predicting the optimal HA design based on input parameters. Sectio 2 2 presents the derivation of the governing equation of the integrated DVA with piezoelectric components. Additionally, it investigates the utilization of a multi-objective weighted sum approach using PSO and GA to determine the optimal parameters of the DVA, with the dual objective of minimizing vibration amplitude and maximizing output voltage. Finally, Section 3 and Section 4 discuss the results and conclusions, respectively.

Methodology

DVA proposed systems

Mathematical modeling

Four DVAs have been proposed with the implementation of the HA and the mechanical inerter to improve the performance of the DVA as illustrated in Figure 1. Only the HA was introduced to the system at the beginning. Then mechanical inerter has been introduced in different configurations to find the best locations. The equation of motion of the four proposed systems is generated.

Propose 1:

$$\boldsymbol{m_1\ddot{X}_1 + Rk_2\left(RX_1 - X_2\right) + k_1X_1 + cR\left(R\dot{X}_1 - \dot{X}_2\right) = Fsin\left(\omega t\right)} \quad (1)$$

$$\boldsymbol{m_2\ddot{X}_2 + k_2\left(X_2 - RX_1\right) + c\left(\dot{X}_2 - R\dot{X}_1\right) + k_3X_2 = 0} \quad (2)$$

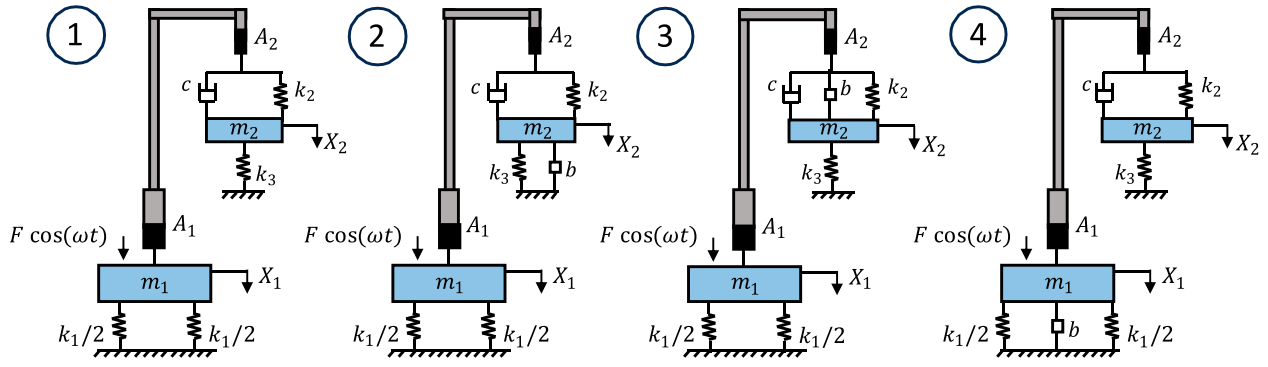

FIGURE 1
Proposed DVA configurations.

Propose 2:

$$m_1\ddot{X}_1 + Rk_2(RX_1 - X_2) + k_1X_1 + cR\left(R\dot{X}_1 - \dot{X}_2\right) = Fsin(\omega t) \quad (3)$$

$$(m_2 + b)\ddot{X}_2 + k_2(X_2 - RX_1) + c\left(\dot{X}_2 - R\dot{X}_1\right) + k_3X_2 = 0 \quad (4)$$

Propose 3:

$$m_1\ddot{X}_1 + bR\left(R\ddot{X}_1 - \ddot{X}_2\right) + Rk_2(RX_1 - X_2) + k_1X_1 + cR\left(R\dot{X}_1 - \dot{X}_2\right) = Fsin(\omega t) \quad (5)$$

$$m_2\ddot{X}_2 + b\left(\ddot{X}_2 - R\ddot{X}_1\right) + k_2(X_2 - RX_1) + c\left(\dot{X}_2 - R\dot{X}_1\right) + k_3X_2 = 0 \quad (6)$$

Propose 4:

$$(m_1 + b)\ddot{X}_1 + Rk_2(RX_1 - X_2) + k_1X_1 + cR\left(R\dot{X}_1 - \dot{X}_2\right) = Fsin(\omega t) \quad (7)$$

$$m_2\ddot{X}_2 + k_2(X_2 - RX_1) + c\left(\dot{X}_2 - R\dot{X}_1\right) + k_3X_2 = 0 \quad (8)$$

In Equations 1–8 m_1 and m_2 denote the masses of the primary and secondary systems, respectively, c represents the damper coefficient, k_1 and k_2 represent the stiffness of the springs in the primary and secondary systems respectively, b is the mechanical inerter coefficient, and R is the amplification ratio A_1/A_2 (A_1 and A_2 are the area of the first and the second piston respectively).

HA analysis

HA is modeled with a circular cross-section tube, and the total loss within the HA is constrained to be less than 10% of the applied force. This constraint was established following a parametric study in the second part of the analysis, which revealed that an increase in the damping coefficient ξ_1 (as depicted in Supplementary Figure S2 of the Supplementary Material) leads to a proportional increase in the vibration amplitude of the primary system. Although the friction loss attributable to oil seals is difficult to quantify, seal manufacturers estimate this loss to range between 1% and 5% (Friction Loss In Hydraulic Cylinder, 2017). For a conservative estimate, a 5% friction loss due to oil seals is assumed. The friction within the HA is modeled as the flow of a Newtonian fluid through a pipe, with the Darcy-Weisbach equation and the Swamee-Jain equation employed for the calculations. The optimized HA is designed to ensure that the total loss remains below 10% of the input force. The relevant Darcy-Weisbach and Swamee-Jain equations are provided below.

$$h = \frac{fLv^2}{2dg} \quad (9)$$

$$f = \frac{1.25}{\left[log\left(\frac{\varepsilon}{3.7d} + \frac{5.74}{Re^{0.9}}\right)\right]^2} \quad (10)$$

where h is the friction loss, f is the friction factor, L is the pipe length, v is the fluid velocity, d is the pipe inner diameter, g is the gravitational constant, Re is the Reynolds number, and ε is the friction coefficient of the pipe, which is assumed to be $45x10^{-6}$ m (typical for commercial-grade piping). The HA illustration is shown in Figure 2. Then DE was used to optimize the diameters (D_1) and lengths (L_1 and L_2) in Equations 9, 10 to obtain the minimum friction loss and the minimum pipe weight. The input parameters which are selected randomly each time between specific ranges are the vibration force (250–1000N), the velocity of the primary system (1–4 m/s), the kinematic viscosity of the hydraulic oil (10^{-6}–$10^{-3}m^2/s$), the amplification ratio ($R \geq 2$), and the total length (1–4m). The optimization process is iterated 10 times, with each iteration employing varied mutation factors and crossover probabilities. The optimal solution is then determined from these iterations. The stopping criteria for each run is to match the maximum number of generations, which is 300.

Following the flowchart in Figure 3, the optimized dataset is filtered to exclude penalty results. Initially, a reduction in inputs and outputs is initiated, where vibration forces are multiplied by the velocity to derive a single input (power). Additionally, a ratio is computed between D_1 and L_2, as well as between L_1 and L_2. This process resulted in streamlining the network to four inputs (Power, kinematic viscosity, pipe length, and amplification ratio) and two outputs (D_1/L_2 and L_1/L_2). After that, all data were normalized by rescaling the values to a range between 0 and 1. Then, the normalized data are trained using an ANN (70% training and 30% testing). An extensive analysis followed, involving varied configurations of ANN layers and neurons, along with testing different sample sizes to identify the best ANN configuration with minimal error. The absolute error is chosen as the error metric, calculated by subtracting the target data (testing data) from the trained data for each iteration. A total of 750 iterations are investigated with a different number of samples, hidden layers, and neurons in each run. The optimal ANN is identified at iteration number 128, achieving a minimum absolute error of 0.3, as depicted in Figure 4.

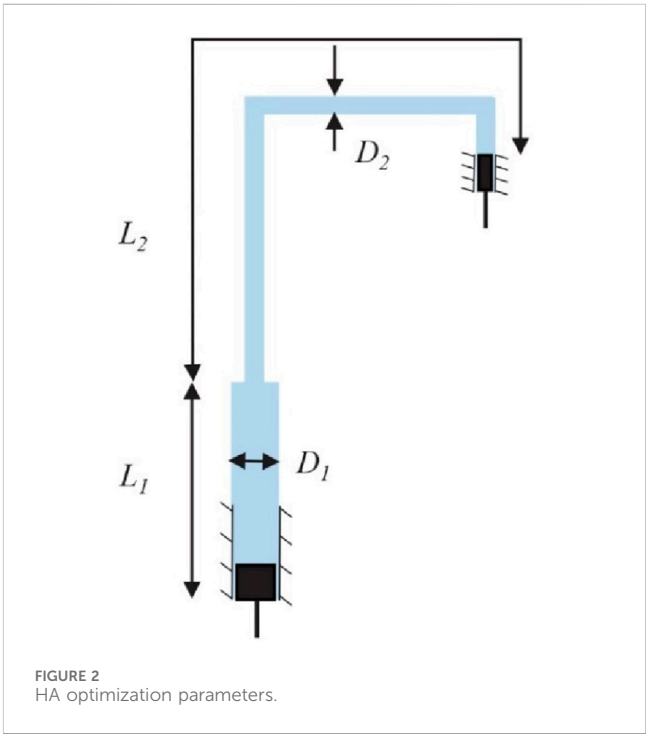

FIGURE 2
HA optimization parameters.

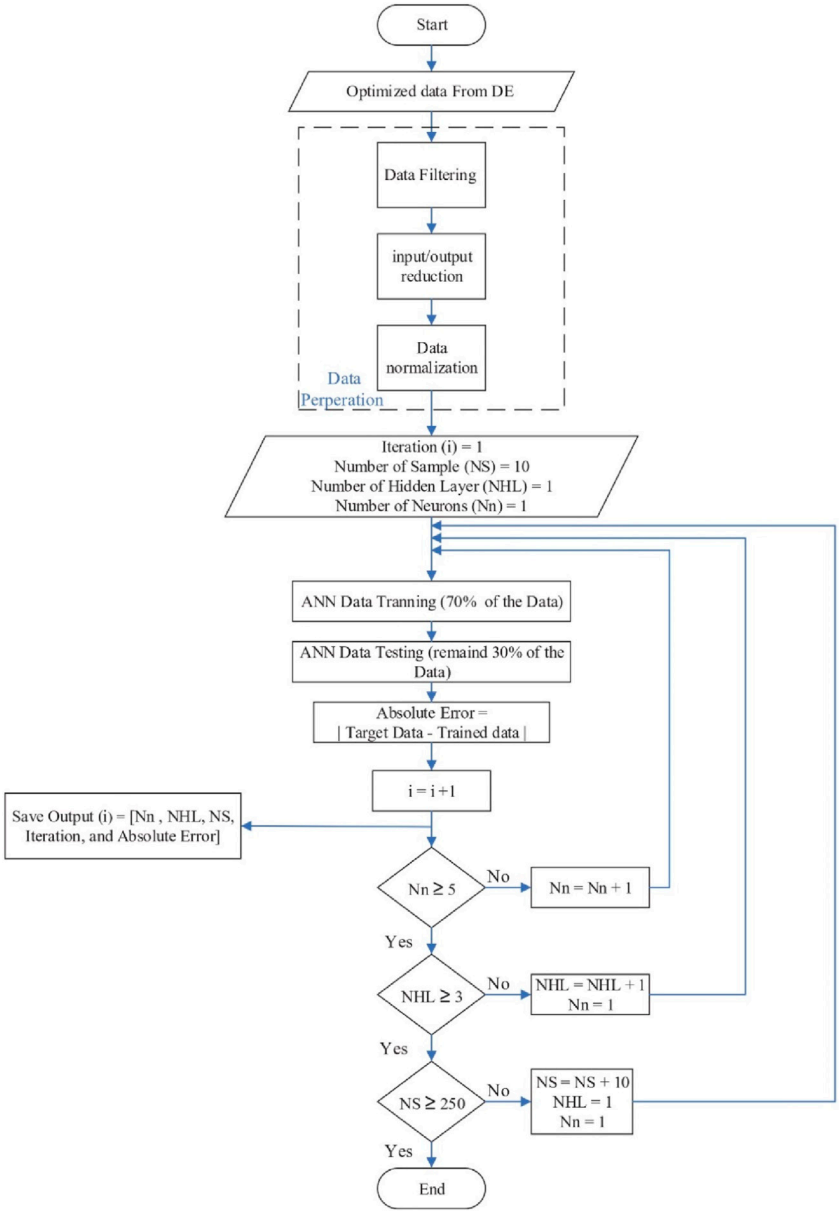

FIGURE 3
DE and ANN methodology flow chart.

The chosen ANN configuration consisted of 560 patterns, featuring 2 hidden layers with 3 hidden neurons each, as delineated in Figure 5.

DVA multi-objective optimization

The second proposed system was used for the analysis. Then, the piezoelectric material is attached to the secondary mass for energy harvesting. The equation of motion of DVA after attaching the piezoelectric material are:

$$m_1\ddot{X}_1 + Rk_2(RX_1 - X_2) + k_1X_1 + cR\left(R\dot{X}_1 - \dot{X}_2\right) = Fsin(\Omega t) \quad (11)$$

$$(m_2 + b)\ddot{X}_2 + k_2(X_2 - RX_1) + c\left(\dot{X}_2 - R\dot{X}_1\right) + k_3X_2 - v\theta_1 = 0 \quad (12)$$

$$c_p\dot{v} + \frac{v}{R} + \theta_2\dot{X}_2 = 0 \quad (13)$$

where θ_1, and θ_2 are the mechanical electrical coupling of the piezoelectric material. After that, the Equation 11–13 have been transferred into dimensionless form. The dimensionless equations are:

$$\ddot{x}_1 + x_1 + R\mu\beta^2(Rx_1 - x_2) + \xi_1(R\dot{x}_1 - \dot{x}_2) = f_0\,sin(\omega\tau) \quad (14)$$

$$\ddot{x}_2 + (x_2 - Rx_1) + \xi_2(\dot{x}_2 - \dot{x}_1) + \alpha x_2 - Qv = 0 \quad (15)$$

$$\dot{v} + \lambda v + k\dot{x}_2 = 0 \quad (16)$$

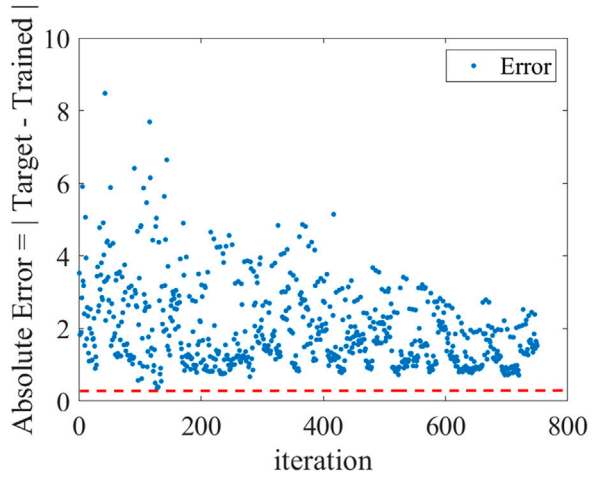

FIGURE 4
Absolute error of the train data.

where x is the normalized dimensionless displacement excitation, and v is the normalized dimensionless voltage. The dimensionless parameters are:

$$\mu = \frac{m_2}{m_1}, \beta = \frac{\omega_{n2}}{\omega_{n1}}, \omega_{n1} = \sqrt{\frac{k_1}{m_1}}, \omega_{n2} = \sqrt{\frac{k_2}{m_2}}, \xi_2 = \frac{R\,c}{(m_2+b)}\sqrt{\frac{k_2}{m_2+b}},$$
$$\xi_1 = \frac{R\,c}{m_1\omega_1}, f_0 = \frac{F}{k_1 x_s} \quad \xi_2 = \frac{c}{(m_2+b)}\sqrt{\frac{k_2}{m_2+b}}, \xi_1 = \frac{c}{m_1\omega_1},$$
$$f_0 = \frac{F}{k_1 x_s}, \tau = \frac{t}{t_s}, \alpha = \frac{k_3}{k_2}, x = \frac{X}{X_s}$$

The dimensionless parameters have been optimized using PSO and GA, the number of populations was set to 20, and the stopping criteria were defined as reaching the maximum number of generations (equal to 100 generations). The study integrates two objective functions: minimizing the maximum vibration amplitude and maximizing the output voltage. The output voltage is calculated as the average value over the study dimensionless frequency range (0.5–1.5). The weight sum optimization method is employed for the multi-objective optimization process. This approach converts the multiple objectives into a single objective, thereby transforming the problem into a minimization or maximization scenario. In this study, energy harvesting is considered a secondary objective, while vibration reduction serves as the primary objective. Consequently, the minimum weight for the primary objective is set at 0.5. The weight sum method is utilized with varying weights assigned to the primary objective (w_1 = 0.5, 0.6, 0.7, 0.8, 0.9, and 1), aiming to minimize the maximum vibration amplitude, and weights assigned to the secondary objective (w_2 = 0.5, 0.4, 0.3, 0.2, 0.1, and zero), targeting the maximization of the average output voltage.

$$\boldsymbol{ObjectiveFunction} = \boldsymbol{w_1} * \boldsymbol{min}\ (\boldsymbol{Maximum}(\boldsymbol{x_1})) - \boldsymbol{w_2} * (\boldsymbol{Mean}(\boldsymbol{v})) \quad (17)$$

where w_1 and w_2 represent the weights of the primary and the secondary objective respectively. Parametric studies of the system parameters were conducted to obtain their influence on the vibration amplitude and output voltage of the system and to specify the range of the parameter values for the multi-objective optimization. The parametric studies of the system parameters are available in the (Supplementary Material). Figure 6 shows the convergence sample of weight sum PSO (inertia weight = 1.4, cognitive parameter = 2, social parameter = 2, and decrement constant = 0.99) and GA (tournament probability = 1, crossover probability = 0.8, mutation probability = 0.05, b = 2, and elite solution = 2) optimizations with w_1 = 0.8 and w_2 = 0.2. Despite the implementation of a GA with 2 elite solutions, the curve exhibits fluctuations. These fluctuations arise from the normalization process carried out within each generation.

Results and discussion

DVA analysis results

The four proposed systems are compared with different R values as illustrated in Figure 7. At R = 1, systems 3 and 4 exhibit the

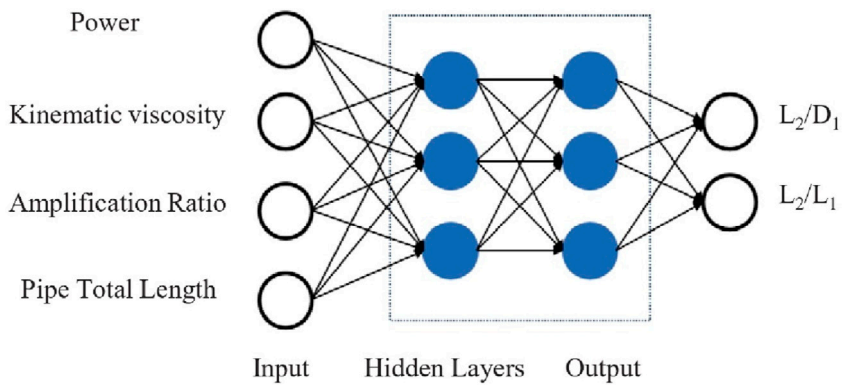

FIGURE 5
Best neural network configuration.

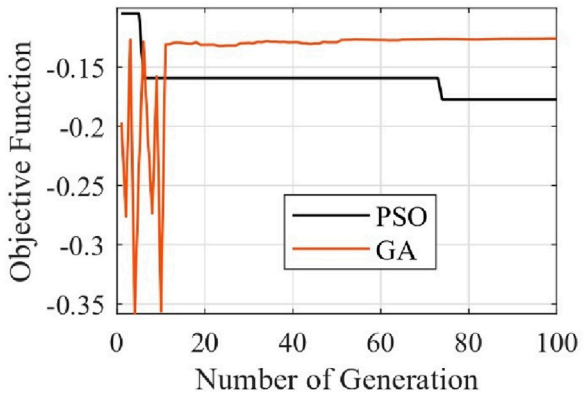

FIGURE 6
PSO and GA weight sum convergence sample (w_1 = **0.8** and w_2 = **0.2**).

highest maximum vibration amplitudes, which are nearly identical. At the resonance frequency ($\omega = 1$) of the primary system, system 3 demonstrates the lowest amplitude, while other systems show similar amplitudes near $\omega = 1$. When $R = 1.5$, the frequency of maximum vibration for all systems shifts to the left, with system 3 displaying the highest amplitude. Notably, system 4 experiences a 20% reduction in maximum vibration amplitude, whereas systems 1 and 2 demonstrate negligible changes. At $\omega = 1$, all systems experience a decrease in vibration amplitude, anticipated due to the amplification process, and the amplitude gap between proposal 3 and others increases. At $R = 2$, the maximum vibration excitation of system 3 increases, alongside leftward shifts in the systems' frequencies. At $\omega = 1$, the system's amplitude is nearly equivalent, and the frequency range exhibiting low amplitudes is expanded, thereby extending the operational frequency range. This results in reducing vibration across a broader range compared to $R = 1$ and 1.5. As R further increases, systems continue to follow a general trend, with leftward shifts in maximum amplitude-frequency and expansions in the working frequency band. Proposal 2 consistently exhibits the lowest maximum amplitude for varying R.

ANN results

The ANN model depicted in Figure 5 serves as a predictive tool for determining the design parameters of the HA (L_1, L_2, and D_1). Through testing with 80 samples from data not utilized in the training phase, the ANN's performance is evaluated. Figures 8, 9

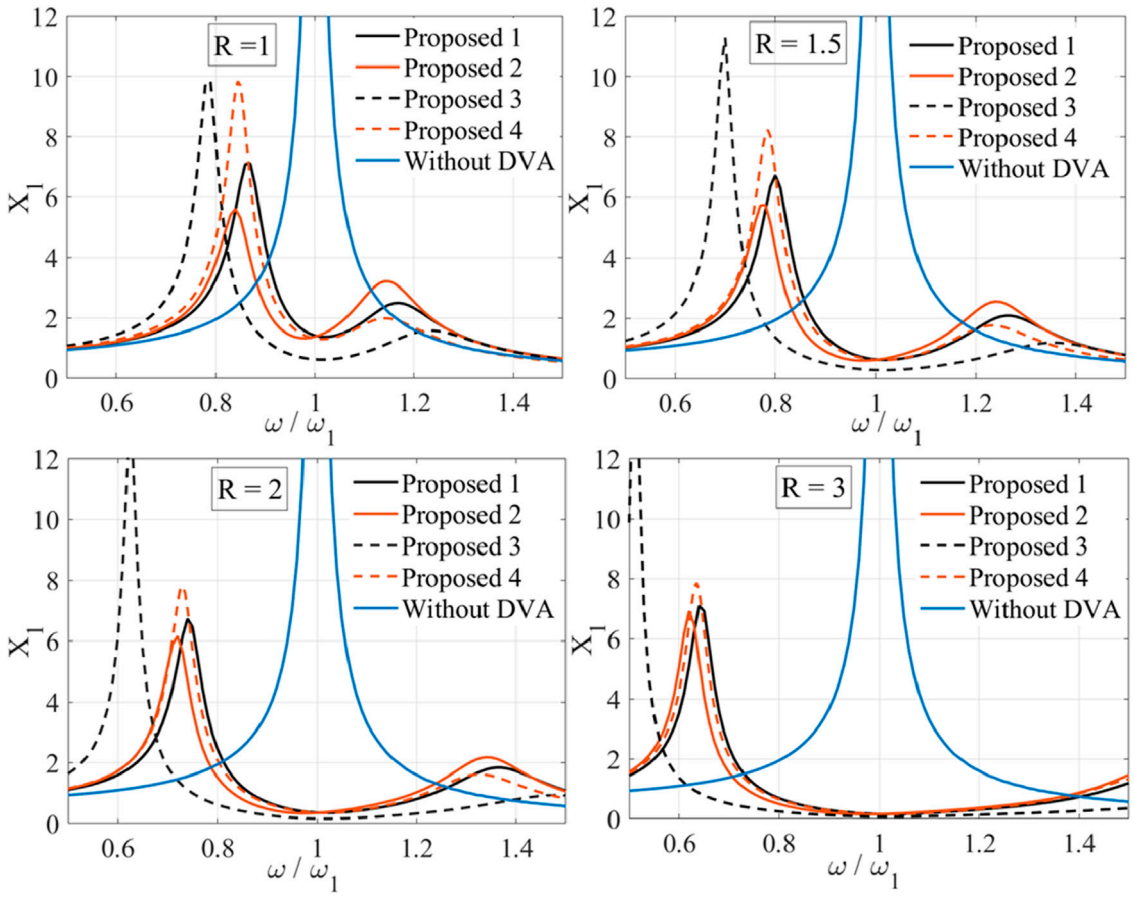

FIGURE 7
System frequency-response of the proposed systems for different R.

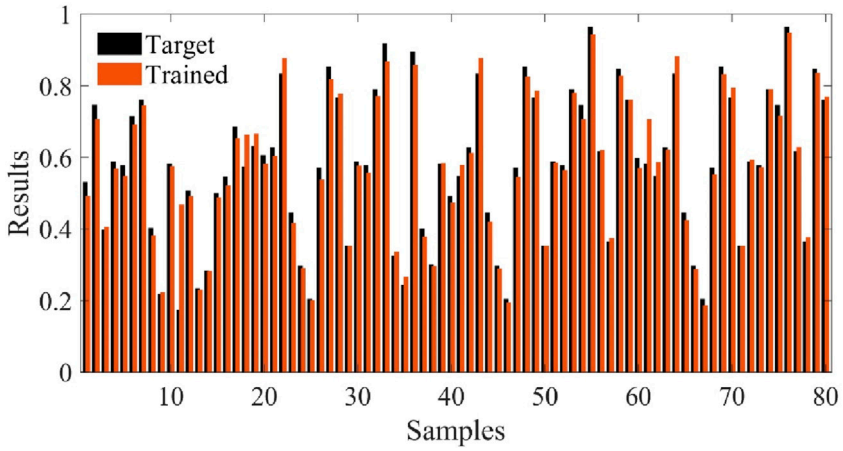

FIGURE 8
L_1/L_2 trained and target results.

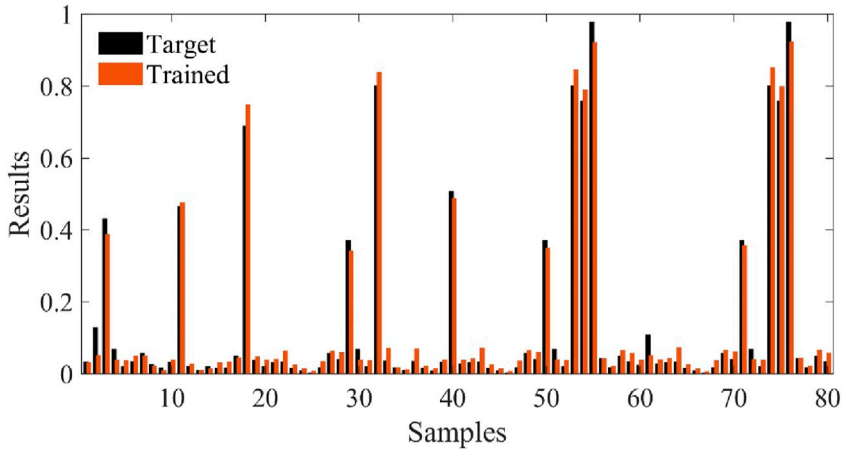

FIGURE 9
D_1/L_2 trained and target results.

present the outputs of the tested samples for L_1/L_2 and L_1/D_1, respectively. These figures demonstrate a predominant clustering of values in close proximity, indicating a high level of agreement between the predicted and actual values. However, certain instances reveal significant errors, highlighting the inherent variability in the analysis. Such discrepancies can be attributed to the complex nature of the system under study. While the ANN generally demonstrates robustness in approximating the relationships between inputs and outputs, occasional deviations may occur, particularly in scenarios characterized by complexity.

Multi-objective PSO and GA optimization

The proposed system in Equation 14–16 is optimized to minimize the maximum vibration amplitude and maximize the average output voltage. The weight sum method with different weights using PSO and GA is used for the optimization. The vibration amplitude of the primary system and the output voltage of the optimized system with different weights are illustrated in Figure 10. The black circles and the red stars represent the optimization points of PSO and GA respectively. Since the step value of ω controls the optimization's computation time a value of increments of ω equal to 0.1 is used throughout the analysis. The solid red and black lines are drawn through quadratic interpolation between these points. The optimal values obtained from the optimization process are summarized in Tables 1, 2. The values of parameters β, α, f_0, and μ are set at 1, 0.02, 0.7, and 0.1, respectively, to achieve these results.

To compare PSO and GA in this multi-objective problem, the Pareto front is conducted for the two techniques. The Pareto front which contains the best solutions is illustrated in Figure 11.

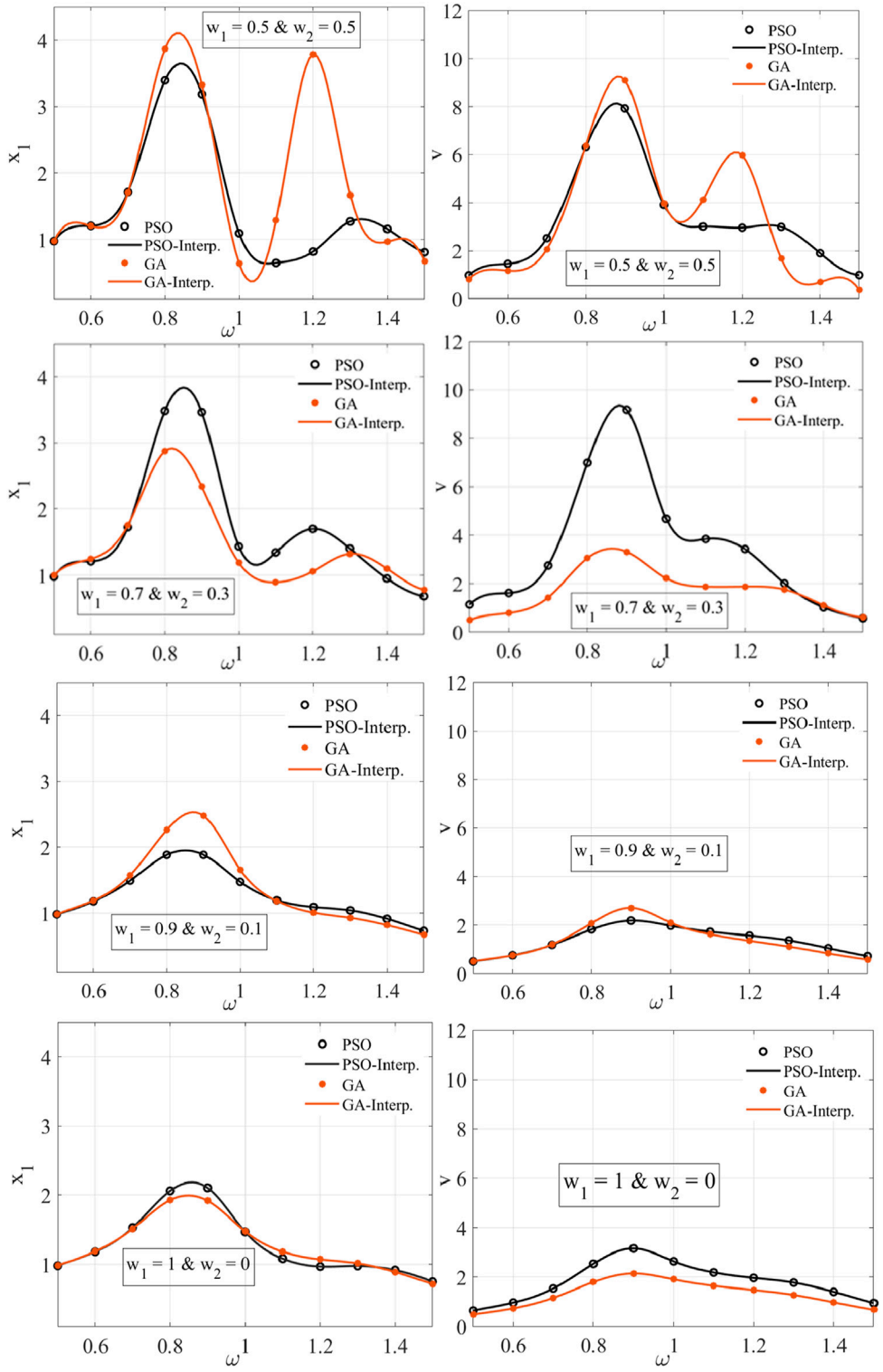

FIGURE 10
PSO and GA frequency-response results of x_1 and v for different weights: optimization points (black circles PSO–red stars GA) and quadratic interpolation (solid line red PSO–solid line black GA).

TABLE 1 PSO multi-objective optimized parameters for different weights.

w_1	w_2	R	ζ_1	ζ_2	λ	Q	k	Max (x_1)	Mean (v)
0.5	0.5	2.56	0.10	0.13	0.56	0.58	0.52	3.40	3.20
0.6	0.4	1.61	0.10	0.18	0.02	0.18	0.60	3.90	3.80
0.7	0.3	1.62	0.10	0.30	0.02	0.16	0.60	3.50	3.40
0.8	0.2	2.77	0.10	0.24	0.81	0.64	0.60	2.80	2.80
0.9	0.1	3.00	0.10	0.10	2.00	1.94	0.60	1.90	1.30
1.0	0.0	3.00	0.10	0.10	1.49	1.44	0.60	2.10	1.80

TABLE 2 GA multi-objective optimized parameters for different weights.

w_1	w_2	R	ζ_1	ζ_2	λ	Q	k	Max (x_1)	Mean (v)
0.5	0.5	1.20	0.10	0.10	0.02	0.10	0.55	3.87	3.30
0.6	0.4	2.93	0.15	0.21	0.80	0.78	0.44	3.40	2.20
0.7	0.3	2.43	0.10	0.11	1.23	1.01	0.45	2.88	1.70
0.8	0.2	2.96	0.11	0.29	1.16	1.51	0.39	2.50	1.34
0.9	0.1	2.96	0.11	0.29	1.16	1.51	0.39	2.50	1.34
1.0	0.0	2.98	0.11	0.11	1.99	1.96	0.58	1.94	1.20

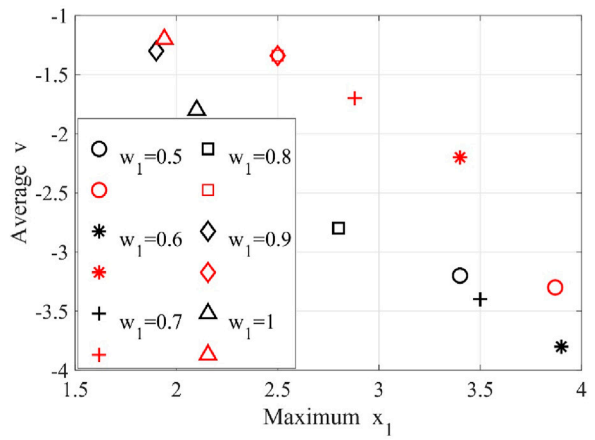

FIGURE 11
Pareto front for PSO and GA multi-objective.

The results show that the multi-objective optimization using PSO gives a better solution than GA in general. The results manifest as nondominated between PSO and GA with the same weights.

Notably, an additional observation emerges regarding the stability of PSO solutions with weight trends, revealing fluctuations in PSO compared to GA solutions under corresponding weight settings as illustrated in Figures 12, 13. Moreover, a general trend surfaces where PSO yields more diverse solutions relative to GA, exemplified by the presence of two repeated solutions at w_1 values of 0.9 and 0.8. These findings are attributed to the inherent complexity of the optimization problem at hand and the heightened sensitivity of parameters, which exert a pronounced influence on the optimization objectives.

Additionally, the existence of resonance constraints within the problem and intricacies in the simulation steps contribute to the observed nuances in the optimization analyses.

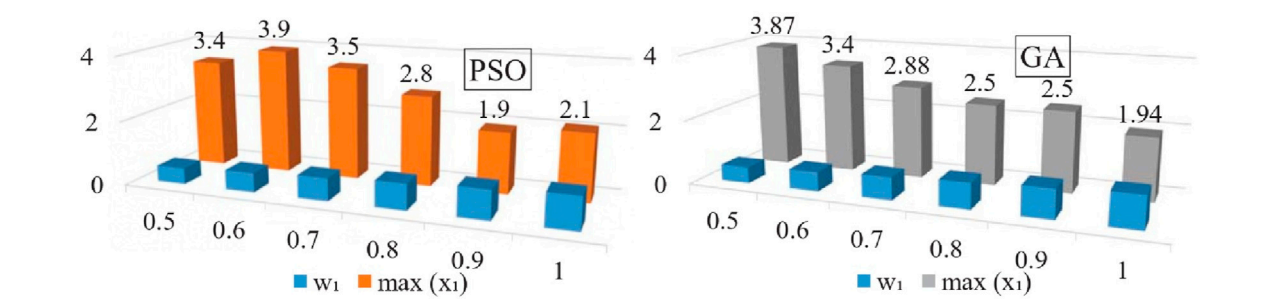

FIGURE 12
Max x_1 in PSO and GA with different weights.

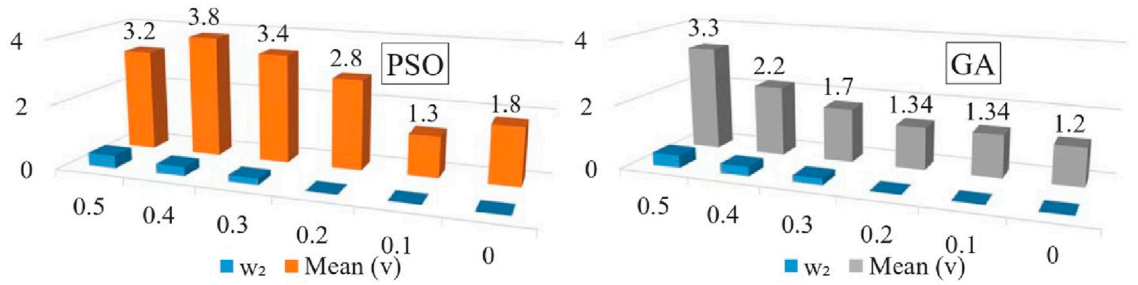

FIGURE 13
Mean v in PSO and GA with different weights.

Conclusion

The proposed model of the DVA incorporating an HA and a mechanical inerter effectively mitigates the limitation imposed by the mass ratio necessary to enhance attenuation. Additionally, it broadens the operational frequency range of the DVA. Also, it has been found that the location of the mechanical inerter is critical in reducing vibration amplitude. The proposed HA design systematically addresses the issue of power loss, and the training data from the ANN successfully facilitates the selection of optimal HA dimensions for various input parameters, achieving a maximum friction loss of less than 10% of the vibration force. In terms of optimization, the multi-objective PSO generally surpasses Genetic Algorithms GA in both diversity and quality of solutions. However, fluctuations in stability have been observed in the PSO weighted sum due to the system's complexity. Therefore, PSO is recommended for future optimization processes in multi-objective vibration system applications.

The characteristics of the DVA with the HA and mechanical inerter proposed in this study make it suitable for a wide range of vibration suppression applications in structural engineering, automotive engineering, and industrial equipment. However, certain limitations of the proposed system must be considered during selection. These include the higher cost compared to lever mechanisms, the need for regularly scheduled maintenance, and the time response limitation, which must be factored into the design. This system is typically better suited for applications involving low-frequency vibrations.

This study demonstrates the effectiveness of meta-heuristic optimization techniques in optimizing complex systems. Future research should include experimental analyses of DVA with HA in vibrating machines and explore the design of an integrated system that connects a single DVA with vibrating equipment.

Data availability statement

The raw data supporting the conclusions of this article will be made available by the authors, without undue reservation.

Author contributions

AS: Conceptualization, Formal Analysis, Investigation, Methodology, Software, Validation, Writing–original draft, Writing–review and editing. MA: Conceptualization, Methodology, Project administration, Supervision, Writing–review and editing. AA: Conceptualization, Methodology, Supervision, Writing–review and editing.

Funding

The author(s) declare that no financial support was received for the research, authorship, and/or publication of this article.

Acknowledgments

The authors would like to acknowledge the support provided by the Interdisciplinary Research Center for Sustainable Energy Systems, (IRC-SES), Research Institute, KFUPM, through project #INRE2328. MA also acknowledges the support received from the Saudi Data and AI Authority (SDAIA) and KFUPM under SDAIA-KFUPM Joint Research Center for Artificial Intelligence Grant no. JRC-AI-RFP-09.

Conflict of interest

The authors declare that the research was conducted in the absence of any commercial or financial relationships that could be construed as a potential conflict of interest.

Publisher's note

All claims expressed in this article are solely those of the authors and do not necessarily represent those of their affiliated organizations, or those of the publisher, the editors and the reviewers. Any product that may be evaluated in this article, or claim that may be made by its manufacturer, is not guaranteed or endorsed by the publisher.

Supplementary material

The Supplementary Material for this article can be found online at: https://www.frontiersin.org/articles/10.3389/fmech.2024.1464692/full#supplementary-material

References

Ahmad, M. F., Isa, N. A. M., Lim, W. H., and Ang, K. M. (2022). Differential evolution: a recent review based on state-of-the-art works. *Alexandria Eng. J.* 61, 3831–3872. doi:10.1016/J.AEJ.2021.09.013

Ahmad, M. M., and Khan, F. U. (2021). Review of vibration-based electromagnetic–piezoelectric hybrid energy harvesters. *Int. J. Energy Res.* 45, 5058–5097. doi:10.1002/ER.6253

Alotta, G., and Failla, G. (2021). Improved inerter-based vibration absorbers. *Int. J. Mech. Sci.* 192, 106087. doi:10.1016/J.IJMECSCI.2020.106087

Arthur, C. K., Temeng, V. A., and Ziggah, Y. Y. (2020). A Self-adaptive differential evolutionary extreme learning machine (SaDE-ELM): a novel approach to blast-induced ground vibration prediction. *SN Appl. Sci.* 2, 1845–1923. doi:10.1007/s42452-020-03611-3

Auleley, M., Thomas, O., Giraud-Audine, C., and Mahé, H. (2021). Enhancement of a dynamic vibration absorber by means of an electromagnetic shunt. *J. Intell. Mater Syst. Struct.* 32, 331–354. doi:10.1177/1045389X20957097/

Baduidana, M., and Kenfack-Jiotsa, A. (2022). Parameters optimization and performance evaluation for the novel tuned inertial damper. *Eng. Struct.* 250, 113396. doi:10.1016/J.ENGSTRUCT.2021.113396

Balaji, P. S., and Karthik SelvaKumar, K. (2020). Applications of nonlinearity in passive vibration control: a review. *J. Vib. Eng. Technol. 2020* 9, 183–213. doi:10.1007/S42417-020-00216-3

Barredo, E., Mendoza Larios, J. G., Colín, J., Mayén, J., Flores-Hernández, A. A., and Arias-Montiel, M. (2020). A novel high-performance passive non-traditional inerter-based dynamic vibration absorber. *J. Sound. Vib.* 485, 115583. doi:10.1016/J.JSV.2020.115583

Bartnicki, A., and Klimek, A. (2019). The research of hydraulic pressure intensifier for use in electric drive system. *IEEE Access* 7, 20172–20177. doi:10.1109/ACCESS.2019.2897148

Bilal, Pant, M., Zaheer, H., Garcia-Hernandez, L., and Abraham, A. (2020). Differential Evolution: a review of more than two decades of research. *Eng. Appl. Artif. Intell.* 90, 103479. doi:10.1016/J.ENGAPPAI.2020.103479

Brötz, N., Rexer, M., Puff, N., and Pelz, P. F. (2024). Fluid dynamic vibration absorber for vehicle suspension system. *Veh. Syst. Dyn.* 62, 1122–1141. doi:10.1080/00423114.2023.2223325

Friction Loss In Hydraulic Cylinder, (2017). Available at: https://iphco.in/learn/learn/learn/friction-loss-in-hydraulic-cylinder/ (Accessed August 14, 2024).

Gad, A. G. (2022). Particle swarm optimization algorithm and its applications: a systematic review. *Archives Comput. Methods Eng. 2022* 29, 2531–2561. doi:10.1007/S11831-021-09694-4

Jangid, R. S. (2021). Optimum tuned inerter damper for base-isolated structures. *J. Vib. Eng. Technol.* 9, 1483–1497. doi:10.1007/s42417-021-00309-7

Kassem, M., Yang, Z., Gu, Y., and Wang, W. (2021). Modeling and control design for flutter suppression using active dynamic vibration absorber. *J. Vib. Eng. Technol.* 9, 845–860. doi:10.1007/s42417-020-00267-6

Kim, N., Kim, S., and Lee, J. (2019). Vibration-based damage detection of planar and space trusses using differential evolution algorithm. *Appl. Acoust.* 148, 308–321. doi:10.1016/J.APACOUST.2018.08.032

Li, J., Gao, T., Zhu, S., and Yang, X. (2023). H∞ optimization of a novel Maxwell dynamic vibration absorber with lever, inerter, and grounded stiffness. *Appl. Sci.* 13, 3697. doi:10.3390/APP13063697

Li, J., Gu, X., Zhu, S., Yu, C., and Yang, X. (2022). Parameter optimization for a novel inerter-based dynamic vibration absorber with negative stiffness. *J. Nonlinear Math. Phys.* 29, 280–295. doi:10.1007/s44198-022-00042-z

Martins, L. A., Lara-Molina, F. A., Koroishi, E. H., and Cavalini, A. A. (2020). Optimal design of a dynamic vibration absorber with uncertainties. *J. Vib. Eng. Technol.* 8, 133–140. doi:10.1007/s42417-019-00084-6

Muscat, A., Bhattacharya, S., and Zhu, Y. (2022). Electromagnetic vibrational energy harvesters: a review. *Sensors (Basel)* 22, 5555. doi:10.3390/S22155555

Qin, Z., Wu, Y. T., He, L., Gao, X., and Lyu, S. K. (2023). Empirical research on the friction behavior of O-rings in hydraulic cylinders. *PLoS One* 18, e0280815. doi:10.1371/JOURNAL.PONE.0280815

Rong, K., Yang, M., Lu, Z., Zhang, J., Tian, L., and Wu, S. (2024). Energy analysis of a nonlinear gas-spring dynamic vibration absorber subjected to seismic excitations. *J. Build. Eng.* 89, 109253. doi:10.1016/J.JOBE.2024.109253

Shami, T. M., El-Saleh, A. A., Alswaitti, M., Al-Tashi, Q., Summakieh, M. A., and Mirjalili, S. (2022). Particle swarm optimization: a comprehensive survey. *IEEE Access* 10, 10031–10061. doi:10.1109/ACCESS.2022.3142859

Shen, Y., Xing, Z., Yang, S., and Sun, J. (2019). Parameters optimization for a novel dynamic vibration absorber. *Mech. Syst. Signal Process* 133, 106282. doi:10.1016/J.YMSSP.2019.106282

Shi, A., Shen, Y., and Wang, J. (2022). Parameter optimization of a grounded dynamic vibration absorber with lever and inerter. *J. Low Freq. Noise Vib. Act. Control* 41, 784–798. doi:10.1177/14613484211068250

Song, Q. H., Xiao, L. J., Song, Q. J., Jiang, H. Y., and Liu, X. J. (2022). Adaptive multiswarm particle swarm optimization for tuning the parameter optimization of a three-element dynamic vibration absorber. *Mech. Sci.* 13, 505–517. doi:10.5194/MS-13-505-2022

Su, N., Bian, J., Chen, Z., and Xia, Y. (2023). A novel lever-type inerter-based vibration absorber. *Int. J. Mech. Sci.* 254, 108440. doi:10.1016/J.IJMECSCI.2023.108440

Sun, R., Zhou, S., and Cheng, L. (2023). Ultra-low frequency vibration energy harvesting: mechanisms, enhancement techniques, and scaling laws. *Energy Convers. Manag.* 276, 116585. doi:10.1016/J.ENCONMAN.2022.116585

Wang, D., Tan, D., and Liu, L. (2017). Particle swarm optimization algorithm: an overview. *Soft Comput.* 22 (2), 387–408. doi:10.1007/S00500-016-2474-6

Wang, M., Xu, H., He, D., Wang, T., and Zhang, J. (2022). Design of a damped vibration absorber to control the resonant vibration of roll. *Mech. Syst. Signal Process* 178, 109262. doi:10.1016/J.YMSSP.2022.109262

Wang, Q., Zhou, J., Wang, K., Gao, J., Lin, Q., Chang, Y., et al. (2023). Dual-function quasi-zero-stiffness dynamic vibration absorber: low-frequency vibration mitigation and energy harvesting. *Appl. Math. Model* 116, 636–654. doi:10.1016/J.APM.2022.12.007

Wang, X., He, T., Shen, Y., Shan, Y., and Liu, X. (2019). Parameters optimization and performance evaluation for the novel inerter-based dynamic vibration absorbers with negative stiffness. *J. Sound. Vib.* 463, 114941. doi:10.1016/J.JSV.2019.114941

Wang, X., Wu, H., and Yang, B. (2020). Nonlinear multi-modal energy harvester and vibration absorber using magnetic softening spring. *J. Sound. Vib.* 476, 115332. doi:10.1016/J.JSV.2020.115332

Xu, H., Ren, C., He, D., Zhou, B., Wang, Q., Gao, H., et al. (2024). Coupling vibration characteristics and vibration suppression of rolling mill rolls with dynamic vibration absorber. *J. Manuf. Process* 120, 1157–1179. doi:10.1016/J.JMAPRO.2024.04.066

Xu, Y., Zhou, H., Zhu, S., and Pan, G. (2021). Research on a hydraulic displacement amplifier for a piezoactuator. *J. Phys. Conf. Ser.* 1985, 012043. doi:10.1088/1742-6596/1985/1/012043

Zhang, R., Zhao, Z., Pan, C., Ikago, K., and Xue, S. (2020). Damping enhancement principle of inerter system. *Struct. Control Health Monit.* 27, e2523. doi:10.1002/STC.2523

Zhe-Ming, C., Peng, W., Jiang-Hua, F., and Bao, C. (2019). Application of SA-PSO algorithm in parameter optimization of dynamic vibration absorber. *IOP Conf. Ser. Earth Environ. Sci.* 267, 042174. doi:10.1088/1755-1315/267/4/042174

Zhou, S., Lallart, M., and Erturk, A. (2022). Multistable vibration energy harvesters: principle, progress, and perspectives. *J. Sound. Vib.* 528, 116886. doi:10.1016/J.JSV.2022.116886

Zoka, H., and Afsharfard, A. (2019). Double stiffness vibration suppressor and energy harvester: an experimental study. *Mech. Syst. Signal Process* 121, 1–13. doi:10.1016/J.YMSSP.2018.11.020